arXiv:cond-mat/0303580v1 [cond-mat.str-el] 27 Mar 2003

Spin and superconducting instabilities near a Van Hove singularity

J. González
Instituto de Estructura de la Materia. Consejo Superior de Investigaciones Científicas. Serrano 123, 28006 Madrid. Spain.
(July 29, 2013)

We apply a wilsonian renormalization group approach to the system of electrons in a two-dimensional square lattice interacting near the saddle-points of the band, when the correlations at momentum $\mathbf{Q} \equiv (\pi, \pi)$ prevail in the system. The detailed consideration of the spin degrees of freedom allows to discern the way in which the SU(2) spin invariance is preserved in the renormalization process. Regarding the spin correlations, we find two different universality classes which correspond, in the context of the extended Hubbard model, to having the bare on-site interaction U repulsive or attractive. The first class is characterized by a spin instability which develops through the condensation of particle-hole pairs with momentum $\mathbf{Q}$, with the disappearance of the Fermi line in the neighborhood of the saddle-points. Within that class, the attractive or repulsive character of the nearest-neighbor interaction V dictates whether there is or not a d-wave superconducting instability in the system. For the Hubbard model with just on-site interaction, we show that some of the irrelevant operators are able to trigger the superconducting instability. The naturalness of the competing instabilities is guaranteed by the existence of a range of doping levels in which the chemical potential of the open system is renormalized to the level of the saddle-points. We incorporate this effect to obtain the phase diagram as a function of the bare chemical potential, which displays a point of optimal doping separating the regions of superconductivity and spin instability.

I. INTRODUCTION

During the last years there has been much effort devoted to the study of strongly correlated electron systems. The interest has been maintained by the behavior displayed by the high-T_c copper-oxide compounds since the discovery of their superconductivity 15 years ago [1]. There are a number of features exhibited by these materials that do not fit into the conventional theoretical frameworks. The normal state of the cuprates shows for instance unusual transport properties and, more strikingly, a pseudogap phase in which part of the density of states is lost at the Fermi level while the system remains conducting. It seems that a new paradigm is needed to describe these materials, in the same way as the Fermi liquid picture accounts for the behavior of conventional metals.

From the theoretical point of view, progress has been made during the past decade in understanding the foundations of Landau's Fermi liquid theory and, consequently, the possible deviations that may open the way to a new kind of metallic behavior [2–4]. The most powerful method used in this task has been the renormalization group (RG) approach developed for interacting fermion systems [2]. We have learned from it that the Fermi liquid picture is a very robust description of the metallic state. There are only a few perturbations that may destabilize the Fermi liquid, favoring the formation of states with different types of symmetry breaking. The Fermi liquid represents itself a universality class in which any electron system falls at dimension $D \geq 2$, unless the interaction is sufficiently long-ranged [5–11] or the Fermi surface develops singular points [12].

Soon after the discovery of the high-T_c superconductivity, it was proposed that the presence of nonlinear dispersion near the Fermi line of the copper-oxide layers could be at the origin of the unconventional behavior [13,14]. The fermion systems in a two-dimensional (2D) square lattice have necessarily saddle-points in their band dispersion, which give rise to Van Hove singularities where the density of states diverges logarithmically. In the most common instances, the two inequivalent saddle-points lie at the boundary of the Brillouin Zone, and their hybridization has been proposed to explain the existence of a d-wave order parameter in the superconducting phase [15–19], as observed experimentally. Further investigations have shown that the unconventional transport properties in the normal state may be accounted for by the proximity of the Fermi level to the Van Hove singularity (VHS) in the copper-oxide layers [20–24].

A careful examination of the kinematics near the saddle-points has shown indeed that a superconducting instability with d-wave order parameter arises in the $t-t'$ Hubbard model with bare repulsive interaction [25,26]. The mechanism at work is of the same kind described by Kohn and Luttinger as giving rise to a p-wave pairing instability in the three-dimensional Fermi liquid [27,28], but adapted now to the 2D model with saddle-points near the Fermi line. Other studies have considered in detail the influence of the entire Fermi line in the development of the instabilities of the system [29,30]. They have given further support to the picture of a competition between a spin-density-wave

instability and a pairing instability with d-wave order parameter in the $t-t'$ Hubbard model with the Fermi level at the VHS. More recently, a refined renormalization program has been implemented in Ref. [31] by trying to handle the momentum dependence of the vertex functions in the scaling procedure, what has confirmed the appearance of different phases with symmetry breaking in the spin and the charge sector.

Despite all the results obtained in the system of electrons near the VHS, there are still important obstacles precluding a precise description of the effective theory at low energies. From a technical point of view, the source of the problem is the appearance of infrared singularities in the RG approach after accomplishing the renormalization of the leading logarithm. Some vertex functions, like the four-point interaction with vanishing total incoming momentum at the one-loop level or the electron self-energy at the two-loop level, get $\log^2(\Lambda)$ corrections in terms of the energy cutoff Λ. After applying the standard RG program, the renormalized quantities still contain factors of the form $\log(\Lambda)$. This fact questions the predictability of the theory since the argument of the logarithm has a hidden energy scale, which sets the strength of the corrections. From a formal point of view, the theory becomes nonrenormalizable in the standard RG approach, since the energy cutoff is not the only dimensionful variable that appears in the scaling process.

The problem of the renormalizability of the theory can be best handled by adopting a wilsonian RG approach, in which only the high-energy modes that live at the cutoff Λ are integrated out at each RG step. In the present paper we follow Shankar's RG program for interacting fermion systems [2], which has the advantage of decoupling the renormalization of the BCS channel (with vanishing momentum of the colliding particles) from that of the rest of the channels at the one-loop level.

Moreover, the important feature of the wilsonian approach is that it allows to set free the chemical potential, so that it can readjust itself at each step of integration. The issue of the renormalization of the chemical potential has been discussed in Ref. [2] in the context of Fermi liquid theory, and it reaches great significance when considering the system of electrons near the VHS. The chemical potential cannot be fixed at the singularity from the start, since it is actually the scale needed to regularize the infrared singularities that appear in the standard RG procedure. On the other hand, the final location of the chemical potential relative to the VHS is not arbitrary, since it is a dynamical quantity that scales in a predictable way upon renormalization.

We remark that the renormalization devised in the paper assumes a constant value of the bare chemical potential, instead of a constant particle number of the system. That is, we describe a situation appropriate for an electron system in contact with a charge reservoir, which sets the nominal value μ_0 of the ensemble. The renormalization accounts for the reduction suffered by the effective chemical potential *inside* the electron system due to the repulsive interaction. This description of the electron system at constant nominal chemical potential is most appropriate when dealing with the Cu-O layers of the cuprate superconductors, since it provides a realization of the contact of the 2D layers with the charge reservoir. The conclusion is that a variation in the external chemical potential does not have always a linear correspondence with the variation of the final renormalized value of μ, which is identified with the Fermi energy of the electron system.

The renormalization of the chemical potential makes possible to address the question of the naturalness of the picture in which the Fermi level is fine-tuned to the VHS. The strength of the predicted instabilities depends crucially on the proximity of the Fermi energy to the singularity. This has been the main criticism to the proposals claiming that the features of the copper-oxide materials could be related to the properties of electrons interacting near a VHS. We will show that the chemical potential is renormalized towards the VHS in a certain range of filling levels, in such a way that it may become pinned to the singularity in the low-energy theory. This fact was already anticipated in Refs. [32], [33] and [16], and it has been used to cure the infrared singularities of the electron self-energy in Ref. [21]. In the present paper, we will take into account such an effect to determine in a predictable way the strength of the pairing instability in the system, as a function of the different values of the bare chemical potential.

In the next section we describe the system to which our analysis applies. In Section III we classify the different renormalized vertices that arise by explicit consideration of the spin degrees of freedom. The universality classes of the system are obtained in Section IV, where we also show the way in which the SU(2) spin invariance is preserved along the RG flow. Section V is devoted to establish the properties of the spin instability of the system, while Section VI analyzes the renormalization of the chemical potential to determine the region of the phase diagram in which the superconducting instability prevails. Finally, the last section is devoted to draw the main conclusions of this work.

II. THE MODEL

We take as starting point of our analysis a system of interacting electrons in the 2D square lattice with nearest-neighbor hopping t and next-to-nearest-neighbor hopping t'. The band dispersion of the model is given by

$$\varepsilon(\mathbf{k}) = -2t(cos(k_x) + cos(k_y)) + 4t'cos(k_x)cos(k_y) \tag{1}$$

where we have set the lattice spacing equal to one. Some of the energy contour lines are shown in Fig. 1. The dispersion has two inequivalent saddle-points A and B at the boundary of the Brillouin Zone. In their neighborhood, the energy of the one-particle states can be approximated by the quadratic form

$$\varepsilon_{A,B}(\mathbf{k}) \approx \mp(t \mp 2t')k_x^2 \pm (t \pm 2t')k_y^2 \tag{2}$$

where the momenta k_x and k_y measure now small deviations from A and B.

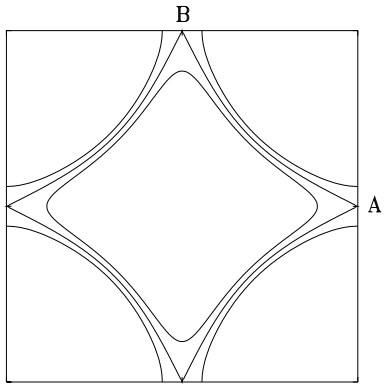

FIG. 1. Contour energy map for the $t - t'$ model about the Van Hove filling.

As a consequence of the nonlinear character of the dispersion, the density of states $n(\varepsilon)$ diverges logarithmically at the level of the saddle-points

$$n(\varepsilon) \approx c \log(t/|\varepsilon|)/(4\pi^2 t) \tag{3}$$

with $c \equiv 1/\sqrt{1-4(t'/t)^2}$. This implies that, when the Fermi level is close to the VHS, most part of the low-energy states are concentrated in the neighborhood of the two saddle-points. In order to apply the RG approach, we may take two patches where the quadratic approximation (2) holds around the saddle-points. Higher-order corrections to the expression (2) are irrelevant under the scaling that makes the action of the model a fixed-point of the RG transformations, as we see in what follows.

We consider then a model whose action at the classical level is

$$\begin{aligned} S = &\sum_a \int dt d^2p \left(i\Psi^+_{a\sigma}(\mathbf{p})\partial_t \Psi_{a\sigma}(\mathbf{p}) - (\varepsilon_a(\mathbf{p}) - \mu_0)\, \Psi^+_{a\sigma}(\mathbf{p})\Psi_{a\sigma}(\mathbf{p}) \right) \\ &+ \sum_{a,b,c,d} \int dt d^2p_1 d^2p_2 d^2p_3 d^2p_4 U(\mathbf{p}_1,\mathbf{p}_2,\mathbf{p}_3,\mathbf{p}_4) \Psi^+_{a\sigma}(\mathbf{p}_1)\Psi^+_{b\sigma'}(\mathbf{p}_2)\Psi_{c\sigma'}(\mathbf{p}_4)\Psi_{d\sigma}(\mathbf{p}_3)\delta(\mathbf{p}_1+\mathbf{p}_2-\mathbf{p}_3-\mathbf{p}_4) \end{aligned} \tag{4}$$

where the indices a, b, c, d run over the two patches around A and B.

The scaling transformation that leaves invariant the kinetic term of the action is

$$\partial_t \to s\partial_t \tag{5}$$

$$\mathbf{p} \to s^{1/2}\mathbf{p} \tag{6}$$

$$\Psi_{a\sigma}(\mathbf{p}) \to s^{-1/2}\Psi_{a\sigma}(\mathbf{p}) \tag{7}$$

It is easily checked that, with the transformation (5)-(7), the interaction term in the action (4) is also scale invariant for a constant value of the potential $U(\mathbf{p}_1,\mathbf{p}_2,\mathbf{p}_3,\mathbf{p}_4)$. If this is not constant, provided that it is a regular function of the arguments we can resort to an expansion in powers of the momenta. Only the constant term is significant, since the rest of higher-order terms fade away upon scaling to the low-energy limit $s \to 0$. This means that we meet the first requirement to apply the RG program, that is to have a model which converges to a fixed-point under RG transformations at the classical level.

In the above scaling, we already find the first deviation in the RG program with respect to the analysis of Fermi liquid theory. In the case of a model with circular Fermi line, the interaction term is scale invariant only for very special kinematics of the scattering processes [2]. In our model, we have seen that no constraint is needed on the four momenta involved in the interaction at the classical level. It is only after taking into account virtual processes that the interactions will start to grow large under scaling for some particular choices of the kinematics. This will

single out a number of so-called marginally relevant channels among all the scattering processes, recovering then the similitude with the analysis of Fermi liquid theory at the quantum level.

The two-patch RG analysis of the $t-t'$ Hubbard model has proven to give the dominant instabilities of the system with the Fermi level at the VHS. For $t' > 0.276\ t$, a ferromagnetic phase has been found below a certain critical frequency [25,26,34,35], in agreement with the results obtained from Monte Carlo calculations [36]. In this paper we will be interested in the regime with $t' < 0.276\ t$, where the competition between a spin instability and a pairing instability arises, making the model more appropriate for the comparison with the phenomenology of the cuprates.

III. WILSONIAN RENORMALIZATION GROUP

In what follows we apply a wilsonian RG approach to obtain the low-energy effective theory of the system. We proceed by progressive integration of the modes in two thin shells of width $d\Lambda$ at distance Λ in energy below and above the Fermi level, as depicted in Fig. 2. For the time being, we will assume that the Fermi level is located precisely at the VHS, unless otherwise stated. This is crucial to obtain a significant renormalization in any of the interaction channels, and later on we will comment on the naturalness of this situation.

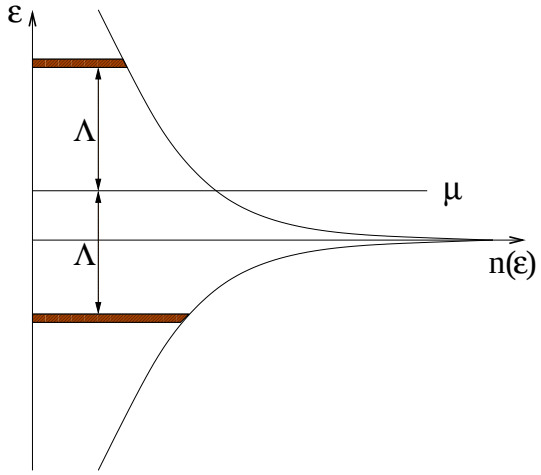

FIG. 2. Picture of the density of states $n(\varepsilon)$ and of the renormalization of the chemical potential μ by integration of states at the energy cutoff Λ.

The vertex functions may become relevant, that is increasingly large at low energies, only for very definite choices of the kinematics. Focusing on the four-point interaction vertex, this is renormalized by a quantity of order $d\Lambda$ at each RG step only when the momentum transfer along a pair of external lines is either $\mathbf{0}$ or $\mathbf{Q} \equiv (\pi, \pi)$, or when the total momentum of the incoming modes vanishes (BCS channel). In the present work we deal with the latter two instances, since the first corresponds to the case of forward-scattering interactions, which are subdominant in the range $t' < 0.276\ t$ that we are considering. In this regime, the divergences at vanishing momentum-transfer are related to charge instabilities of the system, which have been treated in detail elsewhere [37]. We will see that divergences in the channel with momentum transfer $\mathbf{Q}$ give rise to a spin instability, which competes with the superconducting instability in the BCS channel in the model with a bare on-site repulsive interaction.

The different kinematics which may appear in the BCS channel are listed in Fig. 3. We allow for the possibility of Umklapp processes in which the incoming modes scatter from one of the saddle points to the other.

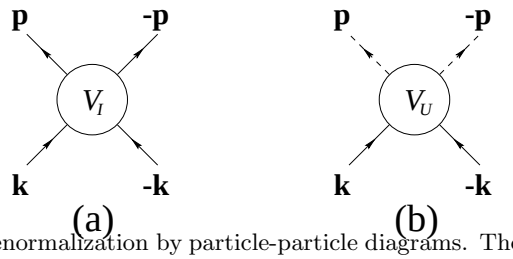

FIG. 3. BCS vertices that undergo renormalization by particle-particle diagrams. The solid and dashed lines stand for modes in the neighborhood of the two different saddle points.

The different kinematical possibilities that arise in the channel with momentum transfer **Q** are classified in Figs. 4 and 5. The first includes the interactions in which the incoming modes are at different saddle points, while the latter contains the Umklapp processes. The other important distinction is between direct (D) and exchange (E) interactions. Direct processes are those in which the momentum transfer **Q** is taken by the same scattered fermion line, while in a exchange process the momentum transfer takes place between two different fermion lines connected only by the interaction.

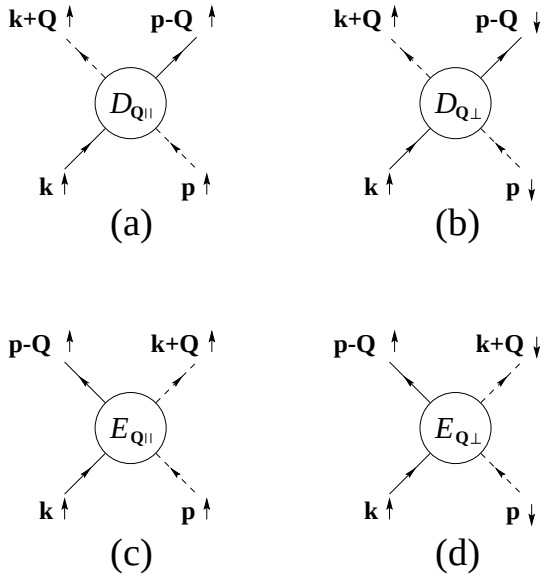

FIG. 4. Direct and exchange vertices that undergo renormalization by particle-hole diagrams.

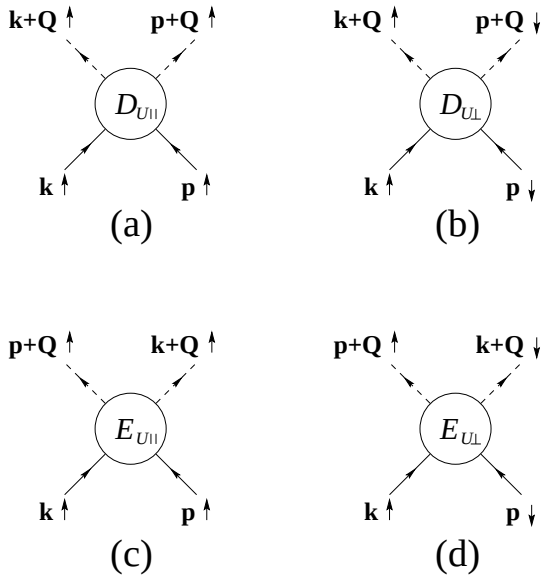

FIG. 5. Umklapp vertices that undergo renormalization by particle-hole diagrams.

The interaction vertices depicted in Figs. 3-5 are all renormalized upon reduction of the cutoff Λ. This can be traced back to the divergent behavior of the different susceptibilities of the model. By integration of the high-energy modes in the shells of width $d\Lambda$, the particle-hole susceptibility at momentum **Q** gets a contribution

$$d\chi_{ph}(\mathbf{Q}) = \frac{c'}{4\pi^2 t} d\Lambda/\Lambda \tag{8}$$

where $c' \equiv \log\left[\left(1+\sqrt{1-4(t'/t)^2}\right)/(2t'/t)\right]$ [38]. In the same fashion, the contribution to the particle-particle susceptibility at zero total momentum is

$$d\chi_{pp}(\mathbf{0}) = \frac{c}{4\pi^2 t}\log(\Lambda)d\Lambda/\Lambda \tag{9}$$

In the latter case, the result of the differential integration diverges logarithmically in the limit $\Lambda \to 0$. This has been a source of problems in the usual RG analyses of the model. The definition of the argument in the logarithm needs an additional scale, while a proper RG scaling requires that the energy is the only dimensionful variable in the problem. It has to be realized that the coefficient at the right-hand-side of Eq. (9) represents actually the density of states. This has to be born in mind for the correct implementation of the RG approach, as we will discuss later.

Let us deal first with the renormalization of the vertices with BCS kinematics in Fig. 3. At the one-loop level, the vertices V_I and V_U get corrections of order $d\Lambda/\Lambda$ from the diagrams shown in Fig. 6. It is important to realize that these are the only diagrams to be taken into account to first order in $d\Lambda$. There are also corrections from particle-hole diagrams but, as long as the momentum that goes into the particle-hole loop is not precisely zero or $\mathbf{Q}$, these terms are of order $(d\Lambda)^2$ and therefore irrelevant in the low-energy limit, as shown graphically in Fig. 7.

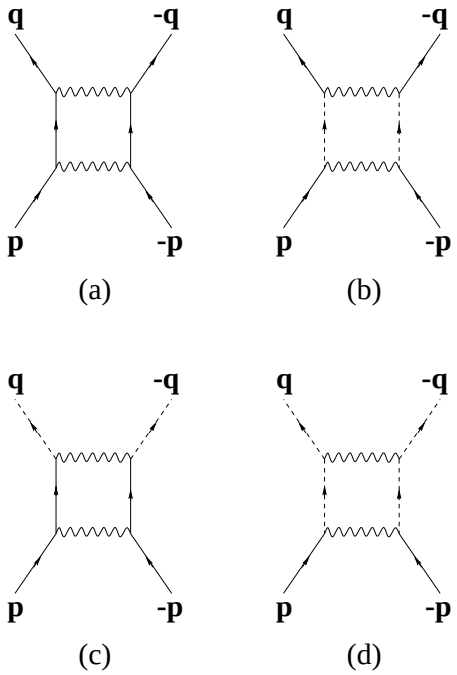

FIG. 6. Particle-particle diagrams renormalizing the BCS vertices at the one-loop level.

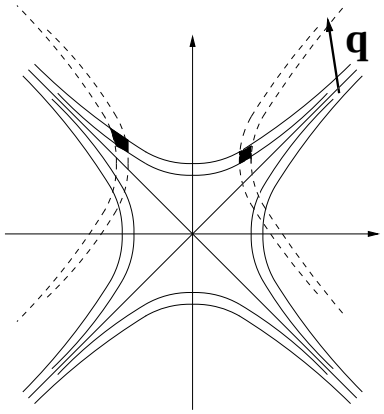

FIG. 7. Picture of the high-energy shells of width $d\Lambda$ at a given saddle-point. The dark regions represent the contribution to a particle-hole diagram when $\mathbf{q}$ is the total incoming momentum.

The BCS vertices mix between themselves alone at the one-loop level, and the situation is similar in that respect to the general analysis of the 2D Fermi liquid [2]. The degree of renormalization depends on the density of states

$n(\varepsilon)$ at the shells integrated out. For later use, we consider at this point the most general case in which the chemical potential μ does not coincide from the start with the level of the VHS. The differential RG equations take then the form

$$\Lambda \frac{\partial V_I}{\partial \Lambda} = c\, n(\mu - \Lambda)\ \left(V_I^2 + V_U^2\right) \tag{10}$$

$$\Lambda \frac{\partial V_U}{\partial \Lambda} = 2c\, n(\mu - \Lambda)\, V_I V_U \tag{11}$$

These equations were considered in Ref. [25], and they also appear as the leading order in the RG approach of Ref. [31].

We consider next the renormalization of the vertices $E_{\mathbf{Q}\perp}$ and $E_{U\perp}$, which have also the property that they mix only between themselves in the one-loop corrections linear in $d\Lambda$. These have been represented in Fig. 8. It can be checked that any other diagrams give irrelevant contributions of order $(d\Lambda)^2$, because they involve either a particle-hole susceptibility at momentum different from $\mathbf{Q}$ or a particle-particle susceptibility with total momentum different from zero. In the latter case, for instance, it is shown in Fig. 9 that the number of intermediate states produced by integration of high-energy modes is quadratic, instead of linear in $d\Lambda$.

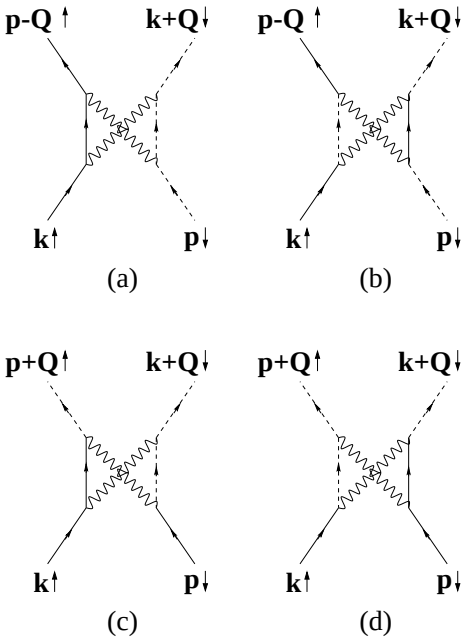

FIG. 8. Particle-hole diagrams renormalizing the vertices $E_{\mathbf{Q}\perp}$ and $E_{U\perp}$ at the one-loop level.

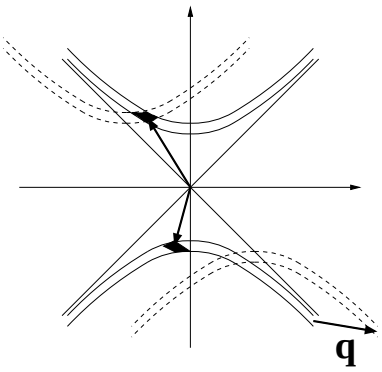

FIG. 9. Same scheme as in Fig. 7. The dark regions represent the contribution to a particle-particle diagram when $\mathbf{q}$ is the total incoming momentum.

The differential RG equations for the pair of vertices read

$$\Lambda\frac{\partial E_{\mathbf{Q}\perp}}{\partial\Lambda} = -c'(E^2_{\mathbf{Q}\perp} + E^2_{U\perp})/(4\pi^2 t) \tag{12}$$

$$\Lambda\frac{\partial E_{U\perp}}{\partial\Lambda} = -c' E_{\mathbf{Q}\perp} E_{U\perp}/(2\pi^2 t) \tag{13}$$

These equations were obtained in Ref. [25], where the names U_{inter} and U_{umk} were used instead of $E_{\mathbf{Q}\perp}$ and $E_{U\perp}$ introduced in the present paper. The same equations also arise at the dominant level in the functional renormalization of Ref. [31].

We now turn to the rest of the vertices, $D_{\mathbf{Q}\parallel}$, $D_{\mathbf{Q}\perp}$, $E_{\mathbf{Q}\parallel}$, $D_{U\parallel}$, $D_{U\perp}$ and $E_{U\parallel}$, which renormalize among themselves at the one-loop level. It is clear that the vertices $D_{\mathbf{Q}\parallel}$ and $E_{\mathbf{Q}\parallel}$ cannot be distinguished from each other just by looking at the external legs. The same applies to $D_{U\parallel}$ and $E_{U\parallel}$. At the one-loop level, one can still discern whether the momentum transfer $\mathbf{Q}$ takes place along the same scattered fermion line or not. However, the different corrections have to organize so that the above pairs of vertices enter in the combinations $D_{\mathbf{Q}\parallel} - E_{\mathbf{Q}\parallel}$ and $D_{U\parallel} - E_{U\parallel}$, which are the quantities that make physical sense. In that respect, the situation is similar to what happens with the couplings $g_{1\parallel}$ and $g_{2\parallel}$ in the one-dimensional electron systems [39].

The one-loop renormalization of the vertices provides an explicit proof of the above statement. The vertex $D_{\mathbf{Q}\parallel}$ gets linear corrections in $d\Lambda$ from the diagrams shown in Fig. 10, while $E_{\mathbf{Q}\parallel}$ is renormalized by the diagrams shown in Fig. 11. Their RG equations read then

$$\Lambda\frac{\partial D_{\mathbf{Q}\parallel}}{\partial\Lambda} = c'\left(D^2_{\mathbf{Q}\parallel} + D^2_{\mathbf{Q}\perp} + D^2_{U\parallel} + D^2_{U\perp} - 2D_{\mathbf{Q}\parallel}E_{\mathbf{Q}\parallel} - 2D_{U\parallel}E_{U\parallel}\right)/(4\pi^2 t) \tag{14}$$

$$\Lambda\frac{\partial E_{\mathbf{Q}\parallel}}{\partial\Lambda} = -c'\left(E^2_{\mathbf{Q}\parallel} + E^2_{U\parallel}\right)/(4\pi^2 t) \tag{15}$$

$$\tag{16}$$

These two equations can be combined to be written in terms of the physical vertex,

$$\Lambda\frac{\partial\left(D_{\mathbf{Q}\parallel} - E_{\mathbf{Q}\parallel}\right)}{\partial\Lambda} = c'\left[\left(D_{\mathbf{Q}\parallel} - E_{\mathbf{Q}\parallel}\right)^2 + \left(D_{U\parallel} - E_{U\parallel}\right)^2 + D^2_{\mathbf{Q}\perp} + D^2_{U\perp}\right]/(4\pi^2 t) \tag{17}$$

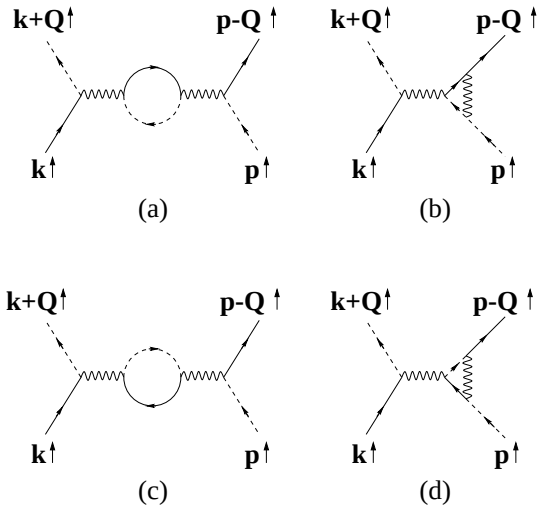

FIG. 10. Particle-hole diagrams renormalizing the vertex $D_{\mathbf{Q}\parallel}$ at the one-loop level.

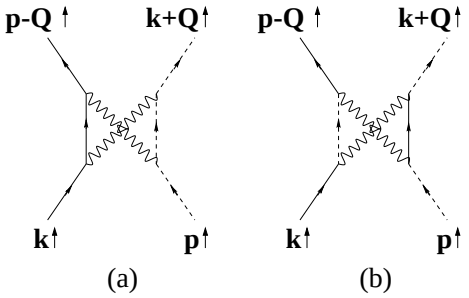

FIG. 11. Particle-hole diagrams renormalizing the vertex $E_{\mathbf{Q}\parallel}$ at the one-loop level.

The RG equations for the remaining vertices also depend on the combinations $D_{\mathbf{Q}\parallel} - E_{\mathbf{Q}\parallel}$ and $D_{U\parallel} - E_{U\parallel}$. In the case of $D_{\mathbf{Q}\perp}$, we have

$$\Lambda \frac{\partial D_{\mathbf{Q}\perp}}{\partial \Lambda} = c' \left[\left(D_{\mathbf{Q}\parallel} - E_{\mathbf{Q}\parallel} \right) D_{\mathbf{Q}\perp} + \left(D_{U\parallel} - E_{U\parallel} \right) D_{U\perp} \right] / (2\pi^2 t) \tag{18}$$

Finally, the RG equations for $D_{U\parallel}$, $D_{U\perp}$ and $E_{U\parallel}$ take the form

$$\Lambda \frac{\partial D_{U\parallel}}{\partial \Lambda} = c' \left(D_{\mathbf{Q}\parallel} D_{U\parallel} - D_{\mathbf{Q}\parallel} E_{U\parallel} - D_{U\parallel} E_{\mathbf{Q}\parallel} + D_{\mathbf{Q}\perp} D_{U\perp} \right) / (2\pi^2 t) \tag{19}$$

$$\Lambda \frac{\partial E_{U\parallel}}{\partial \Lambda} = -c' E_{\mathbf{Q}\parallel} E_{U\parallel} / (2\pi^2 t) \tag{20}$$

$$\Lambda \frac{\partial D_{U\perp}}{\partial \Lambda} = c' \left[\left(D_{\mathbf{Q}\parallel} - E_{\mathbf{Q}\parallel} \right) D_{U\perp} + \left(D_{U\parallel} - E_{U\parallel} \right) D_{\mathbf{Q}\perp} \right] / (2\pi^2 t) \tag{21}$$

As a final check, the equation for $D_{U\parallel} - E_{U\parallel}$ turns out to depend on the physical combination of couplings

$$\Lambda \frac{\partial \left(D_{U\parallel} - E_{U\parallel} \right)}{\partial \Lambda} = c' \left[\left(D_{\mathbf{Q}\parallel} - E_{\mathbf{Q}\parallel} \right) \left(D_{U\parallel} - E_{U\parallel} \right) + D_{\mathbf{Q}\perp} D_{U\perp} \right] / (2\pi^2 t) \tag{22}$$

IV. UNIVERSALITY CLASSES

We discuss now the universality classes in which the system may fall regarding the spin correlations. We will focus on the analysis of bare repulsive interactions, that is where the competition between spin and superconducting instabilities arises. We will see that our RG scheme is able to preserve the spin-rotational invariance of models whose bare interactions have such a symmetry. This provides another nontrivial check of our RG approach, as our framework offers the possibility to analyze the scaling of interactions with and without the SU(2) spin symmetry.

The interactions of physical interest have the property that $D_{\mathbf{Q}\parallel} - E_{\mathbf{Q}\parallel} = D_{U\parallel} - E_{U\parallel}$ and $D_{\mathbf{Q}\perp} = D_{U\perp}$. These conditions are maintained along the RG flow if they are satisfied by the bare couplings. Thus, it is useful to work with the set of couplings

$$D_{\parallel}^{\pm} \equiv D_{\mathbf{Q}\parallel} - E_{\mathbf{Q}\parallel} \pm D_{U\parallel} - E_{U\parallel} \tag{23}$$

$$D_{\perp}^{\pm} \equiv D_{\mathbf{Q}\perp} \pm D_{U\perp} \tag{24}$$

From the results of the preceding section, these new couplings satisfy the equations

$$\Lambda \frac{\partial D_{\parallel}^{\pm}}{\partial \Lambda} = c' \left[(D_{\parallel}^{\pm})^2 + (D_{\perp}^{\pm})^2 \right] / (4\pi^2 t) \tag{25}$$

$$\Lambda \frac{\partial D_{\perp}^{\pm}}{\partial \Lambda} = c' D_{\parallel}^{\pm} D_{\perp}^{\pm} / (2\pi^2 t) \tag{26}$$

The universality classes of the system can be obtained from the integrals of Eqs. (25) and (26). We stick to the case in which $D_{\parallel}^{-} = D_{\perp}^{-} = 0$. The flow for the couplings $D_{\parallel}^{+}$ and $D_{\perp}^{+}$ is represented in Fig. 12. Focusing on interactions that are repulsive at the initial stage of the RG, that is $D_{\parallel}^{+} > 0$ and $D_{\perp}^{+} > 0$, we observe two possible behaviors of

the renormalized couplings. In the case in which the bare couplings satisfy $D_{\parallel}^{+} \geq D_{\perp}^{+}$, the flow is bounded and it converges monotonically to the origin of the space of couplings. If we start otherwise from a point with $D_{\parallel}^{+} < D_{\perp}^{+}$, the flow becomes unstable and it approaches a regime in which $D_{\parallel}^{+} \to -\infty$ and $D_{\perp}^{+} \to +\infty$.

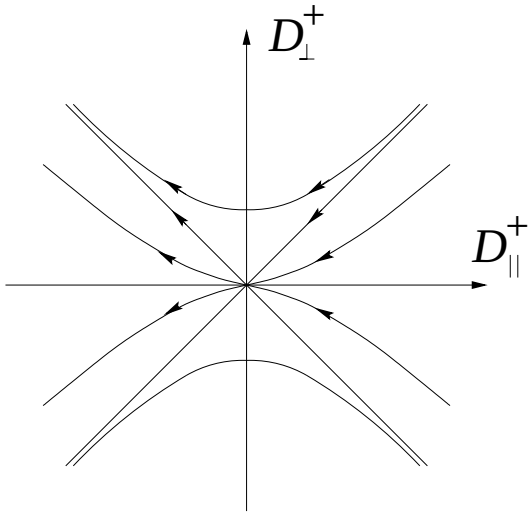

FIG. 12. Flow of the renormalized couplings in the $(D_{\parallel}^{+}, D_{\perp}^{+})$ plane.

The regions with stable and unstable flow correspond to respective universality classes, which imply quite different physical properties. Let us focus, for instance, on the extended Hubbard model with on-site interaction U and interaction V between nearest-neighbor sites. The appropriate bare values for the couplings in Figs. 4 and 5 are

$$D_{\mathbf{Q}\parallel} = D_{\mathbf{Q}\perp} = U - 4V \tag{27}$$
$$E_{\mathbf{Q}\parallel} = E_{\mathbf{Q}\perp} = U + \alpha V \tag{28}$$
$$D_{U\parallel} = D_{U\perp} = U - 4V \tag{29}$$
$$E_{U\parallel} = E_{U\perp} = U - \beta V \tag{30}$$

with $0 < \alpha, \beta < 4$. We have for the initial values of the flow $D_{\parallel}^{+} = -(8 + \alpha - \beta)V$ and $D_{\perp}^{+} = 2U - 8V$. With the physically sensible choice $\alpha = \beta$, we see that the attractive or repulsive character of the on-site interaction dictates whether the RG flow is bounded or not in the upper half-plane of Fig. 12.

The fact that the flow is not bounded for $U > 0$ points to the development of some instability in the system. The divergence of the renormalized couplings represents the failure to describe the model in terms of the original fermion variables. The underlying physical effect is the condensation of boson degrees of freedom, as we will show in the next section. The preservation of the spin-rotational invariance at each step of the RG process helps to clarify the physical interpretation of the instability and to discern the issue of the spontaneous breakdown of the symmetry.

We pay attention then to the way in which the SU(2) spin symmetry is preserved in our RG framework. This can be analyzed by looking at the response functions for the different components of the spin operator. Since the renormalized interactions grow large at momentum transfer $\mathbf{Q} = (\pi, \pi)$, we focus on the correlations of the operator

$$S_j(\mathbf{Q}) = \sum_k \Psi_\sigma^{+}(\mathbf{k} + \mathbf{Q}) \sigma_j^{\sigma\sigma'} \Psi_{\sigma'}(\mathbf{k}) \qquad j = x, y, z \tag{31}$$

The scaling properties of the response functions can be studied in the same fashion as for the interacting one-dimensional fermion systems [40]. The response function $R_z(\omega)$ for the $S_z(\mathbf{Q})$ operator, for instance, is renormalized by the diagrams shown in Fig. 13. After taking the derivative with respect to the cutoff and imposing the self-consistency of the diagrammatic expansion, we obtain

$$\frac{\partial R_z}{\partial \Lambda} = -\frac{2c'}{\pi^2 t}\frac{1}{\Lambda} + \frac{c'}{\pi^2 t}\left(D_{\mathbf{Q}\parallel} - E_{\mathbf{Q}\parallel} + D_{U\parallel} - E_{U\parallel} - D_{\mathbf{Q}\perp} - D_{U\perp}\right)\frac{1}{\Lambda} R_z \tag{32}$$

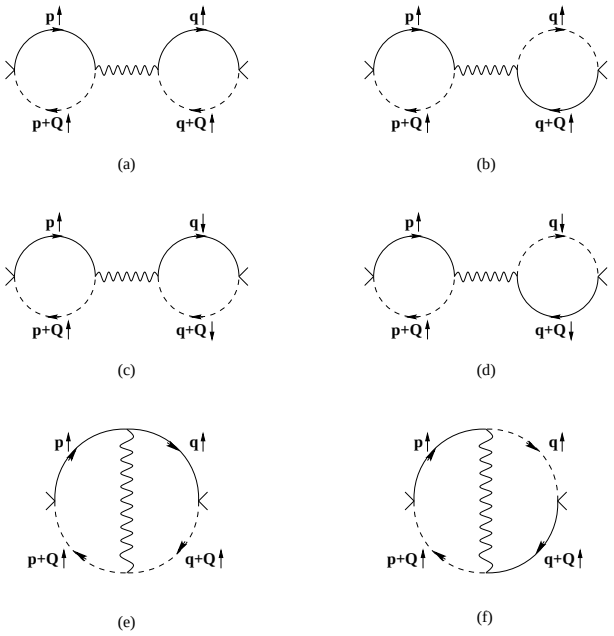

FIG. 13. First-order contributions to the correlator of the S_z operator.

The response functions $R_x(\omega)$ and $R_y(\omega)$ for the other two components of the spin operator are both renormalized by the diagrams shown in Fig. 14. Following the same procedure as for $R_z(\omega)$, we obtain

$$\frac{\partial R_x}{\partial \Lambda} = -\frac{2c'}{\pi^2 t}\frac{1}{\Lambda} - \frac{c'}{\pi^2 t}\left(E_{\mathbf{Q}\perp} + E_{U\perp}\right)\frac{1}{\Lambda}R_x \tag{33}$$

and a completely similar equation for $R_y(\omega)$.

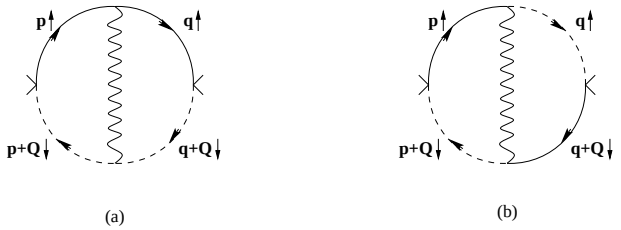

FIG. 14. First-order contributions to the correlators of the S_x and S_y operators.

The response functions $R_x(\omega), R_y(\omega)$ and $R_z(\omega)$ can be made exactly equal if the equation

$$D_{\mathbf{Q}\parallel} - E_{\mathbf{Q}\parallel} + D_{U\parallel} - E_{U\parallel} - D_{\mathbf{Q}\perp} - D_{U\perp} = -E_{\mathbf{Q}\perp} - E_{U\perp} \tag{34}$$

is satisfied all along the flow. From Eqs. (12), (13), (25), and (26), we observe that this is automatically fulfilled when the condition is imposed for the initial values of the couplings. In the case of the extended Hubbard model, we have indeed for the bare couplings in Eqs. (27)-(30)

$$D_{\mathbf{Q}\perp} + D_{U\perp} - D_{\mathbf{Q}\parallel} + E_{\mathbf{Q}\parallel} - D_{U\parallel} + E_{U\parallel} = E_{\mathbf{Q}\perp} + E_{U\perp} = 2U + (\alpha - \beta)V \tag{35}$$

The condition is actually satisfied by the couplings of any hamiltonian that is invariant under rotations. We show in this way that the SU(2) spin symmetry can be preserved at each point of the RG flow of the couplings, so that the low-energy effective action keeps the invariance of the bare hamiltonian.

V. SPIN INSTABILITY

We proceed to determine the physical properties of the universality class corresponding to the unstable flow in the upper half-plane of Fig. 12. The divergence of the renormalized couplings $D_\perp^+ - D_\parallel^+$ and $E_{\mathbf{Q}\perp} + E_{U\perp}$ results

in the divergence of the response functions R_x, R_y and R_z at a certain value of their argument. This points at the development of an instability in the spin sector at the corresponding value of the energy measured from the Fermi level.

The divergence of the response functions implies the existence of a pole at a given frequency ω_c. From the solution to Eqs. (12), (13), (25), and (26), the value of the pole is given by

$$1 - (D_{\perp}^{+}(\Lambda_0) - D_{\parallel}^{+}(\Lambda_0))\chi_{ph}(\mathbf{Q}, \omega_c) = 0 \tag{36}$$

where $D_{\perp}^{+}(\Lambda_0)$ and $D_{\parallel}^{+}(\Lambda_0)$ are the initial values of the couplings. As long as the susceptibility χ_{ph} at momentum $\mathbf{Q}$ diverges logarithmically in the low-frequency limit, it is clear that the above condition is satisfied no matter how small the initial value of the coupling $D_{\perp}^{+} - D_{\parallel}^{+}$ may be.

It is important to bear in mind that the susceptibility χ_{ph} at momentum $\mathbf{Q}$ has a finite imaginary part, which is essential to discern the nature of the ground state of the system. The imaginary part is computed in the Appendix, and it turns out to be $c'/(8\pi t)$. The equation (36) can be written then in the form

$$1 - (D_{\perp}^{+}(\Lambda_0) - D_{\parallel}^{+}(\Lambda_0))\frac{c'}{4\pi^2 t}\log(i\Lambda_0/\omega_c) = 0 \tag{37}$$

which shows that the pole occurs for a pure imaginary value $\omega_c = i|\omega_c|$.

The appearance of a pole in the correlator of a boson operator for a pure imaginary frequency corresponds to a phenomenon of condensation, in the same fashion as it happens in the case of a pairing instability [41]. In the present instance, the boson-like object is the spin operator at momentum $\mathbf{Q}$ defined in Eq. (31). The fact that the pole arises at a value $i|\omega_c|$ means that the instability pertains actually to the theory posed at finite temperature, and that there is a transition to a condensed phase at a temperature of the order of magnitude given by $|\omega_c|$.

In our case, the boson operator that acquires a nonvanishing mean value due to the spin instability is the vector $\int d^2k d\omega \Psi_{\sigma}^{+}(\mathbf{k})\boldsymbol{\sigma}^{\sigma\sigma'}\Psi_{\sigma'}(\mathbf{k}+\mathbf{Q})$. This has important consequences, since the diagrammatic approach has to be rebuilt below the point of the transition, in the same way as in the case of a pairing instability [42].

Let us focus on the Hubbard model, i. e. on a model with interaction between currents with opposite spin projections. To fix ideas, suppose that the vector $\boldsymbol{S}$ gets the nonzero mean value pointing in the x direction. Then, there are two different kinds of one-particle propagators, since the presence of the condensate leads to the consideration of correlators of the type $\langle \Psi_{A\uparrow}^{+}(\mathbf{k},\omega)\Psi_{B\downarrow}(\mathbf{k},\omega)\rangle$, as well as of the usual propagators for well-defined spin projection near each of the saddle-points. To include all the different possibilities, we define the propagator $G_{a\sigma,b\sigma'}(\mathbf{k},\omega)$, with indices a, b labelling the saddle-points and σ, σ' labelling the spin projections:

$$G_{a\sigma,b\sigma'}(\mathbf{k},\omega) = i\langle \Psi_{a\sigma}^{+}(\mathbf{k},\omega)\Psi_{b\sigma'}(\mathbf{k},\omega)\rangle \tag{38}$$

The Schwinger-Dyson equations for the one-particle propagators take the form shown graphically in Fig. 15, where the insertion of the wavy line represents the factor

$$U\int d^2k d\omega \langle \Psi_{A\uparrow}^{+}(\mathbf{k})\Psi_{B\downarrow}(\mathbf{k}+\mathbf{Q})\rangle \equiv \Delta \tag{39}$$

We have, for instance, the closed set of equations

$$G_{A\uparrow,A\uparrow} = G_{A\uparrow,A\uparrow}^{(0)} + G_{A\uparrow,A\uparrow}^{(0)}\Delta G_{B\downarrow,A\uparrow} \tag{40}$$

$$G_{B\downarrow,A\uparrow} = G_{B\downarrow,B\downarrow}^{(0)}\Delta^{*} G_{A\uparrow,A\uparrow} \tag{41}$$

where the superindex 0 denotes the corresponding propagator before the introduction of the condensate. Eqs. (40) and (41) can be combined to give an equation for $G_{A\uparrow,A\uparrow}$, which reads

$$G_{A\uparrow,A\uparrow} = G_{A\uparrow,A\uparrow}^{(0)} + G_{A\uparrow,A\uparrow}^{(0)}\Delta G_{B\downarrow,B\downarrow}^{(0)}\Delta^{*} G_{A\uparrow,A\uparrow} \tag{42}$$

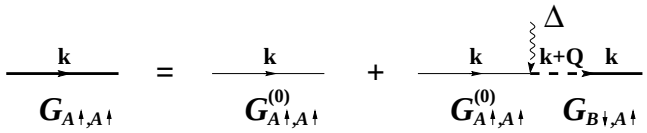

(a)

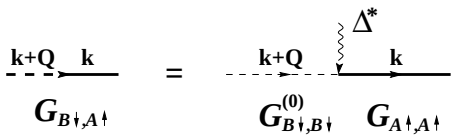

(b)

FIG. 15. Self-consistent equations for the dressed propagators in the particle-hole condensate, in terms of the undressed propagators at the two inequivalent saddle-points.

The solution to Eq. (42) takes the form

$$G_{A\uparrow,A\uparrow}(\mathbf{k},\omega) = \frac{G^{(0)}_{A\uparrow,A\uparrow}(\mathbf{k},\omega)}{1 - G^{(0)}_{A\uparrow,A\uparrow}(\mathbf{k},\omega)|\Delta|^2 G^{(0)}_{B\downarrow,B\downarrow}(\mathbf{k},\omega)} \tag{43}$$

in terms of the propagators at the two different saddle-points

$$G^{(0)}_{A\uparrow,A\uparrow}(\mathbf{k},\omega) = \frac{1}{\omega - \varepsilon_A(\mathbf{k}) + i\epsilon\ \mathrm{sgn}(\omega)} \tag{44}$$

$$G^{(0)}_{B\downarrow,B\downarrow}(\mathbf{k},\omega) = \frac{1}{\omega - \varepsilon_B(\mathbf{k}) + i\epsilon\ \mathrm{sgn}(\omega)} \tag{45}$$

The important point is to determine the pole structure of the propagator (43). Its frequency dependence can be expressed in the form

$$G_{A\uparrow,A\uparrow}(\mathbf{k},\omega) = \frac{\omega - \varepsilon_B(\mathbf{k})}{(\omega - \varepsilon_A(\mathbf{k}) + i\epsilon\ \mathrm{sgn}(\omega))\,(\omega - \varepsilon_B(\mathbf{k}) + i\epsilon\ \mathrm{sgn}(\omega)) - |\Delta|^2} \tag{46}$$

$$= \frac{u(\mathbf{k})^2}{\omega - \varepsilon_u(\mathbf{k}) + i\epsilon\ \mathrm{sgn}(\omega)} + \frac{v(\mathbf{k})^2}{\omega - \varepsilon_v(\mathbf{k}) + i\epsilon\ \mathrm{sgn}(\omega)} \tag{47}$$

with appropriate weights $u(\mathbf{k})^2, v(\mathbf{k})^2$, and $\varepsilon_u(\mathbf{k}), \varepsilon_v(\mathbf{k})$ being the roots of the denominator in Eq. (46)

$$\varepsilon_{u,v}(\mathbf{k}) = \left(\varepsilon_A(\mathbf{k}) + \varepsilon_B(\mathbf{k}) \pm \sqrt{(\varepsilon_A(\mathbf{k}) - \varepsilon_B(\mathbf{k}))^2 + 4|\Delta|^2}\right)/2 \tag{48}$$

From the physical point of view, the most important feature is the appearance of a gap in the quasiparticle spectrum near the saddle-points. This can be checked by determining the shape of the Fermi line, which is given by setting either $\varepsilon_u(\mathbf{k}) = 0$ or $\varepsilon_v(\mathbf{k}) = 0$. Both conditions lead to the equation

$$\varepsilon_A(\mathbf{k})\varepsilon_B(\mathbf{k}) - |\Delta|^2 = 0 \tag{49}$$

By recalling that $\varepsilon_A(\mathbf{k}) = -t_- k_x^2 + t_+ k_y^2$ and $\varepsilon_B(\mathbf{k}) = t_+ k_x^2 - t_- k_y^2$, we end up with the equation satisfied by the points of the Fermi line

$$(t_- k_x^2 - t_+ k_y^2)(t_+ k_x^2 - t_- k_y^2) + |\Delta|^2 = 0 \tag{50}$$

Solving Eq. (50) for the variable k_y^2, for instance, we find that there is a solution only for values of k_x^2 such that

$$(t_+^2 - t_-^2)^2 k_x^4 - 4|\Delta|^2 t_+ t_- \geq 0 \tag{51}$$

Reminding that $t_\pm \approx t \pm 2t'$, this condition implies that, for small values of t', there is a gap in the spectrum of quasiparticles in the range

$$2t'k_x^2 \lesssim |\Delta| \tag{52}$$

We see therefore that the gap opens up in the neighborhood of the saddle-points. The size of the part of the Fermi line destroyed is bounded by $\sqrt{|\Delta|/t'}$, in units of the inverse lattice spacing.

The formation of the quasiparticle gap has its origin in the hybridization of modes at different saddle-points, as a consequence of the enhanced scattering with momentum transfer exactly equal to $\mathbf{Q}$. Quite remarkably, this is an effect that can be studied in the weak coupling regime of the model, and the gap appears for arbitrarily small strength U of the interaction. From the technical point of view, the discussion carried out in this section parallels the treatment of the one-particle Green functions in the usual description of the superconducting instability [42]. However, it is clear that the physical setting is quite different. In the present situation, the condensate is made of particle-hole pairs with a nonvanishing average projection of the spin. The fact that a macroscopic number of these pairs has been formed is what forces the quasiparticles to live out of the range already excited by the condensate.

An important issue concerns the spontaneous breakdown of the spin-rotational symmetry in the condensate. Let us consider the model at zero temperature regarding this matter. It is clear that the nonvanishing average spin cannot have in principle any preferred direction in space. Recalling our definition in Eq. (39), a real value of Δ implies that the spin of the condensate points in the x direction, since

$$\int d^2k d\omega \langle \Psi^+_{A\uparrow}(\mathbf{k}) \Psi_{B\downarrow}(\mathbf{k}+\mathbf{Q}) \rangle + \int d^2k d\omega \langle \Psi^+_{B\downarrow}(\mathbf{k}+\mathbf{Q}) \Psi_{A\uparrow}(\mathbf{k}) \rangle + A \leftrightarrow B = 2(\Delta + \Delta^*)/U \tag{53}$$

A purely imaginary value of Δ implies otherwise that the spin of the condensate lies in the y direction. Finally, it may also be that the nonvanishing mean value is realized for the z component of the spin

$$\int d^2k d\omega \langle \Psi^+_{A\uparrow}(\mathbf{k}) \Psi_{B\uparrow}(\mathbf{k}+\mathbf{Q}) \rangle - \int d^2k d\omega \langle \Psi^+_{A\downarrow}(\mathbf{k}) \Psi_{B\downarrow}(\mathbf{k}+\mathbf{Q}) \rangle + A \leftrightarrow B \neq 0 \tag{54}$$

In the ground state of the model at zero temperature, the spin of the condensate has to point in a definite direction and the SU(2) rotational symmetry is spontaneously broken. As a consequence, two Goldstone bosons arise in the spectrum, which correspond to the spin waves that propagate on top of the particle-hole condensate. These are the gapless excitations of the model, together with the quasiparticle excitations that exist sufficiently far away from the saddle-points.

VI. SUPERCONDUCTING INSTABILITY

We now turn to the instability that arises from the divergent flow of Eqs. (10) and (11). The integral of these equations depends on the position of the chemical potential with respect to the VHS. For this reason, it is crucial to know how μ depends on the cutoff Λ as this is progressively lowered.

The issue of the renormalization of the chemical potential has to be treated necessarily in the framework of the wilsonian RG approach. As the high-energy modes are integrated out at the scale Λ, μ shifts its position by a quantity propotional to $d\Lambda$. At the same time, it is the chemical potential which sets the level to measure the energy cutoff, as shown graphically in Fig. 2. The outcome is that μ adjusts itself at each step of the RG process, until the point in which the cutoff Λ is lowered down to the final chemical potential.

At the computational level, the shift of μ is given by the frequency and momentum-independent part of the electron self-energy, with intermediate states taken from the high-energy modes being integrated. The renormalization is proportional to the charge of the occupied states in the lower slice of width $d\Lambda$, which couples through the forward-scattering vertex F in the usual Hartree and exchange diagrams. The RG equation for the chemical potential reads

$$\frac{d\mu}{d\Lambda} = F(\mu - \Lambda)\, n(\mu - \Lambda) \tag{55}$$

The perturbative approach is further improved by incorporating the renormalization of the F vertex, which bears a well-known dependence on the energy scale measured from the VHS [26,37]

$$F(\varepsilon) \approx F_0/(1 - F_0 \log(|\varepsilon|)/(4\pi^2 t)) \tag{56}$$

When the density of states $n(\varepsilon)$ is a smooth function of the energy, the integration of high-energy modes produces a steady downward flow of μ. The physical interpretation of this effect corresponds to the upward displacement of the one-particle levels due to the repulsive electronic interaction. In the neighborhood of the VHS, the dynamics of μ becomes highly nonlinear given the singular behavior of the density of states in Eq. (55). It turns out that, in

a certain range of initial values, the chemical potential is renormalized down to the VHS and precisely pinned to it in the low-energy regime. As stated in the Introduction, this result pertains to a statistical description in terms of the grand canonical ensemble. The physical picture is appropriate then for an open system in contact with a charge reservoir, which sets the bare value μ_0 of the chemical potential.

In order to evaluate the influence of the VHS on the renormalization of the chemical potential, we have solved Eq. (55) with the approximate density of states

$$n(\varepsilon) = c \log(t/|\varepsilon|)/(4\pi^2 t) \qquad \text{for} \qquad |\varepsilon| \leq 0.5t \tag{57}$$

$$\text{const.} \qquad \text{for} \qquad |\varepsilon| > 0.5t \tag{58}$$

This expression has the correct normalization for the logarithmic singularity in the 2D square lattice. The behavior of the integrals of Eq. (55) with such a density of states is shown in Fig. 16. It is manifest that, for initial values of the chemical potential $\mu_0 \lesssim t$ above the singularity, the final renormalized value of μ lies very close to the VHS. These results are important to assure that the enhancement of the instabilities due to the divergent density of states does not rely on fine-tuning the Fermi level to the VHS, as the chemical potential tends to pin itself in a natural way to the singularity.

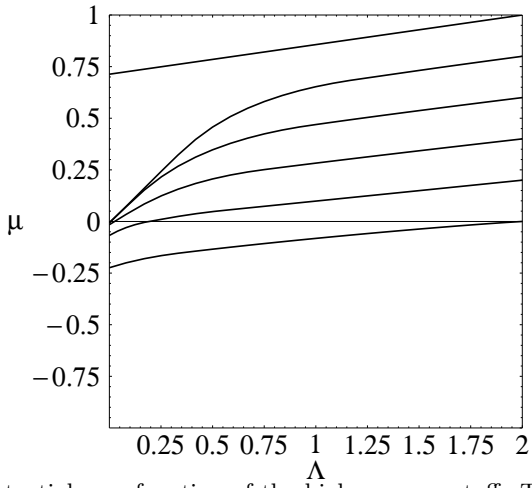

FIG. 16. Scaling of the chemical potential as a function of the high-energy cutoff. The results correspond to the Hubbard coupling $U = 4t$.

The integrals of Eq. (55) can be used now to find the solutions of Eqs. (10) and (11) displaying the superconducting instability. The form of the flow in the coupling constant space is shown in Fig. 17. In the case of bare repulsive interactions, either the BCS couplings scale to zero for $V_I > V_U$, or there is an unstable flow giving rise to the superconducting instability when $V_I < V_U$. The latter instance is realized in lattice models which have a nearest-neighbor attractive interaction V besides the on-site U repulsive interaction. When $V < 0$, the bare coupling $V_I = U + 4V$ is obviously smaller than the bare coupling $V_U = U - 4V$. We are however more interested in the case of the pure Hubbard model, in which the bare couplings lie in the diagonal of the first quadrant in Fig. 17.

The couplings read directly from the hamiltonian of the Hubbard model correspond to the boundary between the regions of stable and unstable flow. This means that the slightest perturbation may drive the system to either of the two sides, which stresses the role played by the irrelevant operators under these conditions. There are actually perturbations that fade away when the theory is scaled to low energies, but that may be important because they may destabilize the flow in the BCS channel.

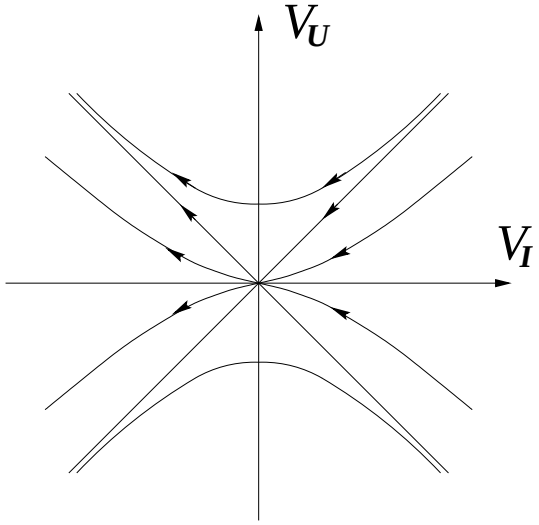

FIG. 17. Flow of the renormalized BCS couplings in the (V_I, V_U) plane.

In the particular case of the Hubbard model, such irrelevant perturbations are given by the iteration of particle-hole diagrams of the type shown in Fig. 18. Apart from the particle-particle diagrams, these are the only corrections that arise from the bare couplings of the model, and they are not enhanced at low energies since the particle-hole bubbles do not have the appropriate kinematics to be of order $\sim d\Lambda$ in the wilsonian approach [2].

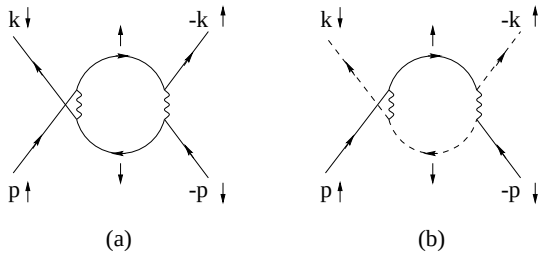

FIG. 18. Particle-hole corrections to the BCS vertices in the Hubbard model.

The iteration of the bubbles in Fig. 18 gives rise to antiscreening diagrams, i. e. to corrections that add to the bare repulsive interaction. We recall that the particle-hole bubble with total momentum about $\mathbf{Q}$ is enhanced with the factor c' given after Eq. (8), while that with momentum about the origin is proportional to the factor c given after Eq. (3). As long as in the present paper we remain in the range $t' < 0.276\, t$, we have that c' is greater than c, and we face the instance in which the irrelevant perturbations make V_U slightly larger than V_I at the beginning of the RG flow.

We have solved the RG equations (10) and (11) taking as initial values for V_I and V_U the result of adding the ladder series built from the diagrams in Fig. 18, with a bare Hubbard coupling $U = 4t$. Moreover, in the resolution we have introduced the dependence of μ on Λ that arises from Eq. (55). This is one of the main accomplishments of our RG procedure, since the knowledge of how the VHS is approached is essential to regularize the effect of the divergent density of states.

The results can be synthesized in the determination of the line at which the transition to the superconducting state takes place in the model. That is characterized by the energy at which the BCS couplings grow large or, more conveniently, by the point at which these couplings have a singularity. This depends on the initial position μ_0 of the chemical potential, and it has been represented as a function of this variable in Fig. 19.

We find that the BCS couplings diverge only for values of μ_0 in the range of attraction to the VHS, that is when the renormalized chemical potential is pinned to the singularity. There is an optimal value of μ_0 for which the scale of the transition reaches a maximum, as the chemical potential stays closer to the VHS during a greater part of the RG flow. For lower values of μ_0, the scale of the instability decreases, as a consequence of the fact that the renormalized chemical potential is not precisely pinned then to the VHS.

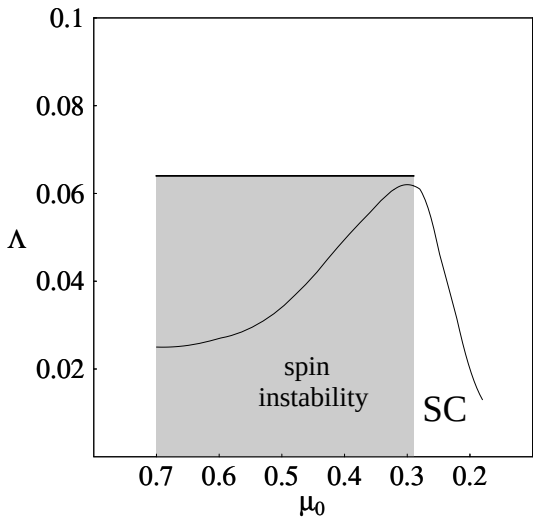

FIG. 19. Plot of the energy scale of the superconducting instability (thin line) and of the transition to the spin instability phase (shaded region).

We have also represented in Fig. 19 the energy at which the spin instability opens up, according to the estimate of Section V. We realize that this scale is always above the energy at which the singularity develops in the BCS channel, whenever the spin instability exists in the system. This happens for values of μ_0 higher than the optimal one. For lower values, the renormalized chemical potential deviates from the VHS by an amount even larger than the gap that would be due to the spin instability, so that this does not find the conditions to develop. We have then a picture in which the pairing instability exists alone for μ_0 below the optimal doping, but it is actually precluded above that level since the spin instability sets in before with the formation of a gap in the quasiparticle spectrum.

We comment finally on the symmetry of the condensate wavefunction. The fact that the Umklapp interaction V_U becomes increasingly repulsive when approaching the instability implies that the wavefunction must have opposite signs in the saddle-points A and B. As long as in the unstable flow we approach the asymptotic regime $V_I = -V_U$, the response function for the d-wave operator

$$\Psi^+_{A\uparrow}(\mathbf{k})\Psi^+_{A\downarrow}(-\mathbf{k}) - \Psi^+_{B\uparrow}(\mathbf{k})\Psi^+_{B\downarrow}(-\mathbf{k}) + \text{h.c.} \tag{59}$$

develops a singularity at the frequency where the coupling $V_I - V_U$ blows up. By the same token, it is easily seen that the response function for the s-wave operator does not display any divergence at low energies. Without the need of knowing precisely the shape of the gap, we may assure then that the symmetry of the order parameter is of d-wave type, with nodal lines at the bisectors of the four quadrants. This is in agreement with the results of more general analyses, which show that the symmetry of the order parameter can be ascertain from the topology of the Fermi line alone [12].

VII. CONCLUSIONS

In this paper we have presented a study of the different phases of the system of electrons interacting near a Van Hove singularity, when the correlations at momentum $\mathbf{Q} \equiv (\pi, \pi)$ prevail over those at zero momentum. In the context of a model with nearest-neighbor and next-to-nearest-neighbor hopping, this happens for $0 < t' < 0.276\, t$, according to the comparison of the prefactors c and c' that appear in Eqs. (3) and (8), respectively. We have applied a wilsonian RG approach following the same lines developed by Shankar in Ref [2] for the analysis of Fermi liquid theory. We have paid attention to the spin degrees of freedom when considering the different interactions, what has allowed us to discern the universality classes of the system.

We have seen that, regarding the spin correlations, there is a universality class characterized by a spin instability in the low-energy theory, in opposition to the regime of couplings with smooth behavior of the correlators for the spin operators. In the case of the extended Hubbard model with on-site interaction U and nearest-neighbor interaction V, the spin instability arises for $U > 0$, irrespective of the value of V, and it is absent for $U < 0$.

Several authors have previously considered the competition between the spin and the superconducting instabilites in the universality class corresponding to the divergent flow in the upper half-plane of Fig. 12 [15,17,25,26,29–31]. Our analysis has shed light into a number of features of the spin instability. We have seen that this takes place through the

condensation of particle-hole pairs with momentum $\mathbf{Q}$. The fact that a macroscopic number of these pairs has been formed is what forces the quasiparticles to live out of the range Δ excited by the condensate in the neighborhood of the saddle-points. The Fermi line is destroyed in a region whose size is bounded by $\sqrt{|\Delta|/t'}$, in units of the inverse lattice spacing.

This effect provides a paradigm for the disappearance of the Fermi surface of an electron system which differs from the understanding of such a phenomenon in Mott-Hubbard insulators. Those systems are supposed to be in a strong-coupling regime, in which the double occupancy of each lattice site is highly suppressed. In our case, we need otherwise to constrain the Fermi level near the VHS, departing sensibly from half-filling as t' is increased. Most remarkably, the instability takes place no matter how small the bare couplings may be in the above picture. This is what ultimately allows to discern the symmetry breaking in the ground state within our RG approach.

We have seen that two different behaviors arise also in the space of couplings for the BCS channel, starting from bare repulsive interactions V_I and V_U. The d-wave superconducting instability develops in models corresponding to the region with unstable flow in the upper half-plane of Fig. 17. This is the case of the extended Hubbard model with $U > 0$ and attractive interaction V. When $U > 0$ and the nearest-neighbor interaction is repulsive, the couplings in the BCS channel scale down to zero. The Hubbard model with just on-site interaction is placed at first sight on the boundary between the regions with stable and unstable behavior. We have shown that the model has irrelevant perturbations that drive the system towards the side with divergent RG flow. Since the departure from the limit behavior is weak, the superconducting instability is overshadowed by the spin instability, up to a point of optimal doping beyond which the latter is absent.

The use of the wilsonian RG approach provides some advantages over other RG methods, the most important being the possibility of studying the renormalization of the chemical potential. Given the divergent behavior of the density of states at the VHS, it is clear that all the positions of the Fermi level cannot be equally stable. The scaling of the chemical potential can be obtained by letting it free to evolve and computing the shift from the integration of high-energy modes near the cutoff at each RG step. Following this procedure, we have seen that there is a range of attraction near the VHS where the chemical potential is renormalized down to the singularity. This guarantees the naturalness of the different instabilities since, rather than relying on the fine-tuning of the Fermi level, they arise from its precise pinning to the VHS in the low-energy effective theory.

APPENDIX

In this section we compute the imaginary part of some of the susceptibilities of the model. It turns out that the particle-hole susceptibility $\chi_{ph}(\mathbf{Q},\omega)$ and the particle-particle susceptibility $\chi_{pp}(\mathbf{0},\omega)$ have a nontrivial imaginary part, while this vanishes for $\chi_{ph}(\mathbf{0},\omega)$ and $\chi_{pp}(\mathbf{Q},\omega)$ at any finite frequency.

In our model, the susceptibility $\chi_{ph}(\mathbf{Q},\omega)$ is given by

$$\chi_{ph}(\mathbf{Q},\omega) = i \int \frac{d\omega_q}{2\pi} \int \frac{d^2q}{(2\pi)^2} \frac{1}{\omega + \omega_q - \varepsilon_A(\mathbf{q}) + i\epsilon\ \mathrm{sgn}(\omega+\omega_q)} \frac{1}{\omega_q - \varepsilon_B(\mathbf{q}) + i\epsilon\ \mathrm{sgn}(\omega_q)} \tag{60}$$

where the energy cutoff is implicit in the integration over the momenta. According to the standard prescription, the imaginary part of (60) is given by

$$\mathrm{Im}\ \chi_{ph}(\mathbf{Q},\omega) = -2\pi^2 \int \frac{d\omega_q}{2\pi} \int \frac{d^2q}{(2\pi)^2} \mathrm{sgn}(\omega+\omega_q)\ \mathrm{sgn}(\omega_q)\ \delta(\omega+\omega_q-\varepsilon_A(\mathbf{q}))\ \delta(\omega_q - \varepsilon_B(\mathbf{q})) \tag{61}$$

In the limit of small t', Eq. (61) leads to a quantity which does not depend on the frequency. Taking $\omega > 0$, we have

$$\mathrm{Im}\ \chi_{ph}(\mathbf{Q},\omega) = \frac{1}{4\pi} \int d^2q\ \delta(\omega + 2t(q_x^2 - q_y^2)) \tag{62}$$

$$= \frac{1}{8\pi t} \int_{-q_0}^{q_0} dq_x \frac{1}{\sqrt{q_x^2 + \omega/(2t)}} \tag{63}$$

where $q_0 = \sqrt{\frac{\omega(t-2t')}{8tt'}}$. After a little of algebra, we obtain

$$\mathrm{Im}\ \chi_{ph}(\mathbf{Q},\omega) = \frac{1}{8\pi t} \log\left(\frac{t}{2t'} + \sqrt{\frac{t^2}{4t'^2} - 1}\right) \tag{64}$$

$$= c'/(8\pi t) \tag{65}$$

We see therefore that the imaginary part is equal to $\pi/2$ times the prefactor of $\log(\Lambda)$ in the real part of the susceptibility. It can be checked that the same relation holds between the real and the imaginary part of the particle-particle susceptibility $\chi_{pp}(\mathbf{0},\omega)$.

Turning now to the susceptibility $\chi_{ph}(\mathbf{0},\omega)$, we have

$$\text{Im } \chi_{ph}(\mathbf{0},\omega) = \text{Re} \int \frac{d\omega_q}{2\pi} \int \frac{d^2q}{(2\pi)^2} \frac{1}{\omega+\omega_q-\varepsilon_A(\mathbf{q})+i\epsilon \text{ sgn}(\omega+\omega_q)} \frac{1}{\omega_q-\varepsilon_A(\mathbf{q})+i\epsilon \text{ sgn}(\omega_q)} \tag{66}$$

$$= -2\pi^2 \int \frac{d\omega_q}{2\pi} \int \frac{d^2q}{(2\pi)^2} \text{sgn}(\omega+\omega_q) \text{ sgn}(\omega_q) \ \delta(\omega+\omega_q-\varepsilon_A(\mathbf{q})) \ \delta(\omega_q-\varepsilon_A(\mathbf{q})) \tag{67}$$

$$= -\frac{1}{4\pi}\delta(\omega) \int d^2q \tag{68}$$

We see then that the imaginary part of the susceptibility is zero for any finite value of the frequency.

A result similar to (68) is obtained for the imaginary part of the susceptibility $\chi_{pp}(\mathbf{Q},\omega)$. In this channel, the pole that arises after summing up the ladder series corresponds to the appearance of excited states in the spectrum. We conclude therefore that the breakdown of symmetry through a mechanism of condensation can only take place in the particle-particle channel at zero momentum and in the particle-hole channel at momentum $\mathbf{Q}$, as stated in the text.

---

[1] See, for instance, E. Dagotto, Rev. Mod. Phys. **66**, 763 (1994), and P. W. Anderson, *The Theory of Superconductivity in the High-T_c Cuprates* (Princeton Univ., Princeton, 1997).

[2] R. Shankar, Rev. Mod. Phys. **66**, 129 (1994).

[3] J. Polchinski in *Proceedings of the 1992 TASI in Elementary Particle Physics*, J. Harvey and J. Polchinski eds. (World Scientific, Singapore, 1992).

[4] W. Metzner, C. Castellani and C. di Castro, Adv. Phys. **47**, 3 (1998).

[5] P.-A. Bares and X.-G. Wen, Phys. Rev. B **48**, 8636 (1993).

[6] J. Gan and E. Wong, Phys. Rev. Lett. **71**, 4226 (1993).

[7] A. Houghton, H.-J. Kwon, J. B. Marston and R. Shankar, J. Phys. Condens. Matter **6**, 4909 (1994).

[8] C. Castellani and C. Di Castro, Physica C **235-240**, 99 (1994). C. Castellani, C. Di Castro and A. Maccarone, Phys. Rev. B **55**, 2676 (1997). C. Castellani, S. Caprara, C. Di Castro and A. Maccarone, Nucl. Phys. B **594**, 747 (2001).

[9] C. Nayak and F. Wilczek, Nucl. Phys. B **417**, 359 (1994).

[10] J. González, F. Guinea and M. A. H. Vozmediano, Nucl. Phys. B **424**, 595 (1994).

[11] S. Chakravarty, R. E. Norton and O. F. Syljuasen, Phys. Rev. Lett. **74**, 1423 (1995).

[12] J. González, F. Guinea and M. A. H. Vozmediano, Phys. Rev. Lett. **79**, 3514 (1997).

[13] J. Labbé and J. Bok, Europhys. Lett. **3**, 1225 (1987). J. Friedel, J. Phys. (Paris) **48**, 1787 (1987); **49**, 1435 (1988). R. S. Markiewicz and B. G. Giessen, Physica **160C**, 497 (1989). C. C. Tsuei *et al.*, Phys. Rev. Lett. **65**, 2724 (1990). D. M. Newns *et al.*, Phys. Rev. Lett. **69**, 1264 (1992).

[14] A review of the Van Hove scenario for high-T_c superconductivity has been made by R. S. Markiewicz, J. Phys. Chem. Sol. **58**, 1179 (1997).

[15] H. J. Schulz, Europhys. Lett. **4**, 609 (1987). P. Lederer, G. Montambaux and D. Poilblanc, J. Phys. (Paris) **48**, 1613 (1987). J. E. Dzyaloshinskii, Pis'ma Zh. Eksp. Teor. Fiz. **46**, 97 (1987) [JETP Lett. **46**, 118 (1987)].

[16] J. González, F. Guinea and M. A. H. Vozmediano, Europhys. Lett. **34**, 711 (1996); report cond-mat/9502095.

[17] L. B. Ioffe and A. J. Millis, Phys. Rev. B **54**, 3645 (1996).

[18] D. Zanchi and H. J. Schulz, Phys. Rev. B **54**, 9509 (1996).

[19] D. Z. Liu and K. Levin, Physica **275C**, 81 (1997).

[20] P. C. Pattnaik *et al.*, Phys. Rev. B **45**, 5714 (1992).

[21] J. González, F. Guinea and M. A. H. Vozmediano, Nucl. Phys. B **485**, 694 (1997).

[22] D. Menashe and B. Laikhtman, Phys. Rev. B **59**, 13592 (1999).

[23] G. Kastrinakis, Physica C **340**, 119 (2000).

[24] V. Yu. Irkhin and A. A. Katanin, Phys. Rev. B **64**, 205105 (2001).

[25] J. V. Alvarez, J. González, F. Guinea and M. A. H. Vozmediano, J. Phys. Soc. Jpn. **67**, 1868 (1998).

[26] J. González, F. Guinea and M. A. H. Vozmediano, Phys. Rev. Lett. **84**, 4930 (2000).

[27] W. Kohn and J. M. Luttinger, Phys. Rev. Lett. **15**, 524 (1965).

[28] For a review, see M. A. Baranov, A. V. Chubukov and M. Yu. Kagan, Int. J. Mod. Phys. B **6**, 2471 (1992).

[29] C. J. Halboth and W. Metzner, Phys. Rev. B **61**, 7364 (2000); Phys. Rev. Lett. **85**, 5162 (2000).

[30] C. Honerkamp, M. Salmhofer, N. Furukawa and T. M. Rice, Phys. Rev. B **63**, 35109 (2001).
[31] B. Binz, D. Baeriswyl and B. Douçot, Eur. Phys. J. B **25**, 69 (2002).
[32] R. S. Markiewicz, J. Phys.: Condens. Matter **2**, 665 (1990).
[33] D. M. Newns, P. C. Pattnaik and and C. C. Tsuei, Phys. Rev. B **43**, 3075 (1991).
[34] V. Yu. Irkhin, A. A. Katanin and M. I. Katsnelson, Phys. Rev. B **64**, 165107 (2001).
[35] C. Honerkamp and M. Salmhofer, Phys. Rev. Lett. **87**, 187004 (2001).
[36] S. Sorella, R. Hlubina and F. Guinea, Phys. Rev. Lett. **78**, 1343 (1997).
[37] J. González, Phys. Rev. B **63**, 45114 (2001).
[38] H. Q. Lin and J. E. Hirsch, Phys. Rev. B **35**, 3359 (1987).
[39] J. Sólyom, Adv. Phys. **28**, 201 (1979).
[40] H. J. Schulz, in *Correlated Electron Systems*, Vol. 9, ed. V. J. Emery (World Scientific, Singapore, 1993).
[41] A. A. Abrikosov, L. P. Gorkov and I. E. Dzyaloshinski, *Methods of Quantum Field Theory in Statistical Physics*, Chap. 7 (Dover, New York, 1975).
[42] E. M. Lifshitz and L. P. Pitaevskii, *Statistical Physics, Part 2*, Chap. 5 (Pergamon Press, Oxford, 1980).